FERMILAB-PUB-06-452-CD

Astronomy & Astrophysics manuscript no. sclanal8s December 4, 2006
(DOI: will be inserted by hand later)

Superclusters of galaxies from the 2dF redshift survey. II. Comparison with simulations

J. Einasto[1], M. Einasto[1], E. Saar[1], E. Tago[1], L. J. Liivamägi[1], M. Jõeveer[1], I. Suhhonenko[1], G. Hütsi[1], J. Jaaniste[2], P. Heinämäki[3], V. Müller[4], A. Knebe[4], and D. Tucker[5]

[1] Tartu Observatory, EE-61602 Tõravere, Estonia
[2] Estonian University of Life Sciences
[3] Tuorla Observatory, Väisäläntie 20, Piikkiö, Finland
[4] Astrophysical Institute Potsdam, An der Sternwarte 16, D-14482 Potsdam, Germany
[5] Fermi National Accelerator Laboratory, MS 127, PO Box 500, Batavia, IL 60510, USA

Received 2006; accepted

Abstract. We investigate properties of superclusters of galaxies found on the basis of the 2dF Galaxy Redshift Survey, and compare them with properties of superclusters from the Millennium Simulation. We study the dependence of various characteristics of superclusters on their distance from the observer, on their total luminosity, and on their multiplicity. The multiplicity is defined by the number of Density Field (DF) clusters in superclusters. Using the multiplicity we divide superclusters into four richness classes: poor, medium, rich and extremely rich. We show that superclusters are asymmetrical and have multi-branching filamentary structure, with the degree of asymmetry and filamentarity being higher for the more luminous and richer superclusters. The comparison of real superclusters with Millennium superclusters shows that most properties of simulated superclusters agree very well with real data, the main differences being in the luminosity and multiplicity distributions.

Key words. cosmology: large-scale structure of the Universe – clusters of galaxies; cosmology: large-scale structure of the Universe – Galaxies; clusters: general

1. Introduction

The largest non-percolating galaxy systems are superclusters of galaxies which contain clusters and groups of galaxies along with their surrounding galaxy filaments. Superclusters evolve slowly and contain information about the very early universe; thus their properties can be used as cosmological probes to discriminate between different cosmological models. Early studies of superclusters were based on galaxies and groups (see the reviews by Oort 1983 and Bahcall 1988). All-sky catalogues of superclusters were complied by Zucca et al. (1993), Kalinkov & Kuneva (1995), Einasto et al. (1994, 1997, 2001, hereafter E01) using galaxy cluster catalogues by Abell (1958) and Abell et al. (1989).

In fact, superclusters consist of galaxy systems of different richness classes – from single galaxies, galaxy groups and filaments to rich clusters of galaxies. This has been realised long ago (Jõeveer, Einasto & Tago 1978, Gregory & Thompson 1978) and has been confirmed by recent studies of superclusters using deep new galaxy surveys, such as the Las Campanas Galaxy Redshift Survey, the 2 degree Field Galaxy Redshift Survey (2dFGRS, Colless et al. 2001, 2003), and the Sloan Digital Sky Survey (SDSS) (Doroshkevich et al. 2001, Einasto et al. 2003a, 2003b; Erdogdu et al. 2004; Porter and Raychaudhury 2005; and Einasto et al. 2006a, hereafter Paper I). These new surveys have shown that morphological properties of galaxies depend on the large-scale cosmological environment: Einasto et al. (2003c, 2003a, 2005b, hereafter E05b); Balogh et al. (2004); Croton et al. (2005a); Lahav (2004 and 2005); Ragone et al. (2004). The densest global environment is provided in superclusters of galaxies.

The goal of this paper is to investigate properties of real superclusters and to compare them with simulated superclusters found in numerical simulations of the evolution of the structure of the Universe. We shall use the supercluster catalogue of Paper I and catalogues of simulated superclusters based on the Millennium Simulation of Springel et al. (2005) (see also Gao et al. 2005 and Croton et al. 2005b). Traditionally in supercluster studies the multiplicity and the shape is discussed and used as a cosmological probe (Basilakos et al. 2001, Kolokotronis et al. 2002, Basilakos 2003, Wray et al. 2006). Additional parameters of galaxy systems in high- and low-density environment (supercluster and field populations) were investigated by Doroshkevich et al. (2001) using the minimal spanning tree and inertia tensor methods. In this paper we shall discuss also a number of supercluster properties, such as the luminosity function; the maximal, minimal and effective diameters and their

Send offprint requests to: J. Einasto

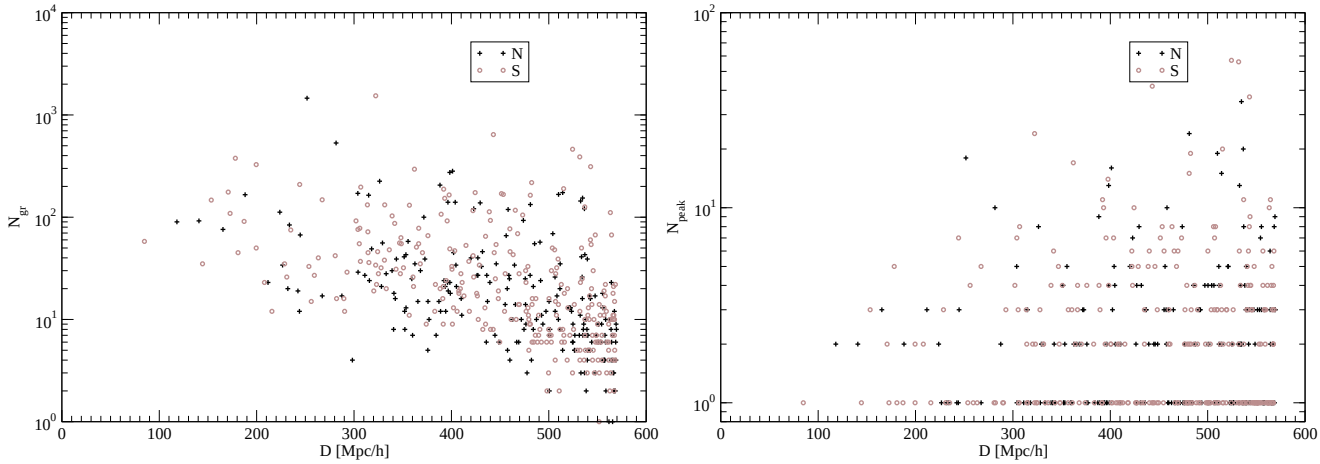

Fig. 1. The multiplicity of superclusters at various distances from the observer. Here we have used groups of galaxies in the left panel and DF-clusters in the right panel as supercluster multiplicity indicators.

ratios; the geometric and dynamical centres and their differences; and the main clusters and galaxies. We define the multiplicity of superclusters by the number of Density Field (DF) clusters, and divide superclusters according to their multiplicity into four richness classes: poor, medium, rich and extremely rich. Properties of galaxies in superclusters, including properties of main galaxies and main clusters, shall be investigated in a separate paper by Einasto et al. (2006c, Paper III).

The paper is composed as follows. Section 2 describes the data used for the analysis. In Section 3 we discuss multiplicities of superclusters and define supercluster richness classes. In Section 4 we study properties of superclusters and compare these properties with those of simulated superclusters. We consider the dependence of supercluster properties on the distance from the observer, on the total luminosity, and on the richness. In Section 5 we discuss our results and compare our lists of superclusters with superclusters found in earlier studies. In the last sections we give our conclusions. The catalogue of superclusters is available electronically at the web-site `http://www.aai.ee/~maret/2dfscl.html`.

2. Data

We have used in this analysis supercluster catalogues published by Einasto et al. (Paper I). The main data used in this paper can be found in the electronic supplement of this paper; some unpublished data on real and model supercluster samples are also used. The main data are the following.

The geometric data are: the supercluster distance d, and the minimal, maximal, and effective diameters of the supercluster, D_{min}, D_{max}, D_e. The minimal diameter is the shortest size of the supercluster along rectangular coordinates x, y, z, calculated in rectangular equatorial coordinates (for details see Paper I), the maximal diameter is the diagonal of the box containing the supercluster along rectangular coordinates, and the effective diameter is the diameter of the sphere whose volume equals that of the supercluster. We further use the ratio of the mean to effective diameter $\epsilon_0 = D_m/D_e$, where $D_m = D_{max}/3^{1/3}$ is the mean diameter. This parameter characterizes the compactness of the system. A further geometrical parameter is the center offset, which is the difference between the geometric center (as defined by the x, y, z-coordinates of the density field above the threshold density), and the dynamic centre, identified with the center of the main (most luminous) cluster of the supercluster. This parameter characterises the asymmetry of the supercluster.

The physical data are: the peak and mean density of the supercluster (in units of the mean luminosity density); the number of galaxies and groups (from the catalogue by Tago et al. 2006, hereafter T06); the multiplicity of the supercluster, defined as the number of DF-clusters in it (for definition of DF-clusters see below Sect. 3); and the total luminosity of the supercluster, L_{tot}, expressed in Solar units in the b_j filter passband. The total luminosity of a supercluster is calculated by summing the estimated total luminosities of its member galaxies and groups.

We use corresponding characteristics for simulated superclusters using the Millennium Simulation by Springel et al. (2005).

3. Multiplicities of superclusters and supercluster richness classes

Peaks of the luminosity density have been calculated using luminosities of groups corrected for the effect of luminosity bias. These data are used to find DF-clusters – peaks of the density field smoothed with an Epanechnikov kernel of radius 8 h^{-1} Mpc. The use of the Epanechnikov kernel is preferable since it has no low-density wings as the Gaussian kernel. The number density of DF-clusters is 57 and 58 per million $(h^{-1}\,\mathrm{Mpc})^3$, respectively, in the 2dFGRS Northern and Southern regions, using a threshold density of 5.0 in units of the mean density. For the Millennium Simulation density field DF-clusters have been found for a density threshold of 5.5; for this limit the number density of DF-clusters is 25 per million $(h^{-1}\,\mathrm{Mpc})^3$. For comparison we note that the number density of Abell clusters is 26 per million $(h^{-1}\,\mathrm{Mpc})^3$ (Einasto et al. 1997). If a higher threshold density is used, then the number density of DF-clusters in 2dFGRS samples becomes very close to the

Table 1. Data on 2dFGRS and Millennium Simulation superclusters of various richness

Name			2dF				Mill		
	Rich	N	1st	med	4nd	N	1st	med	4nd
L_{tot}	P	365	5.157e11	8.302e11	1.347e12	1432	1.554e12	2.425e12	3.962e12
	M	151	1.526e12	2.583e12	4.267e12	283	6.028e12	1.028e13	1.720e13
	R	18	1.055e13	1.528e13	1.866e13	18	2.695e13	3.852e13	4.278e13
	E	9	2.024e13	4.320e13	4.975e13	1		1.048e14	
M_m	P		-20.66	-20.94	-21.30		-22.14	-22.44	-22.77
	M		-20.73	-21.02	-21.34		-22.61	-22.87	-23.13
	R		-21.16	-21.45	-21.74		-23.00	-23.20	-23.42
	E		-21.09	-21.31	-21.57			-23.71	
δ_m	P		5.07	5.37	5.99		5.03	5.36	5.95
	M		5.42	5.89	6.46		5.57	6.14	6.88
	R		6.25	6.90	7.19		6.45	6.71	7.35
	E		6.91	7.26	7.87			7.35	
δ_p	P		5.140	5.780	7.330		5.200	5.930	7.533
	M		5.675	6.740	9.070		5.880	8.190	11.840
	R		8.643	10.400	12.460		10.26	11.72	16.81
	E		11.07	12.29	16.33		11.33	11.33	11.33
D_{max}	P		13.93	17.49	21.95		14.07	18.22	23.69
	M		27.81	34.07	42.61		31.49	41.68	53.00
	R		75.61	84.56	90.48		73.80	85.32	106.30
	E		93.11	126.40	153.90			136.4	
D_e	P		7.51	9.58	11.70		7.71	9.87	12.20
	M		12.21	14.82	17.70		13.80	16.66	19.88
	R		24.90	27.10	28.49		23.30	25.96	27.24
	E		29.73	39.44	40.90			36.68	
Δ_o	P		2.39	3.41	4.33		1.57	2.55	4.06
	M		5.05	6.59	8.70		5.42	8.27	12.50
	R		13.2	15.2	23.5		13.6	23.49	27.89
	E		15.5	19.2	23.4			26.26	
ϵ_0	P		1.02	1.06	1.12		1.02	1.06	1.15
	M		1.26	1.33	1.49		1.32	1.44	1.58
	R		1.65	1.77	1.83		1.79	1.96	2.13
	E		1.81	1.95	2.22			2.15	

Millennium Simulation and Abell cluster density estimates. In other words, DF-clusters can be considered as an equivalent to Abell clusters. We searched the neighbourhood of DF-clusters for galaxies and groups of galaxies. This search shows that all DF-clusters lie in a high-density environment: in a box of radius 3 h^{-1} Mpc around a DF-cluster there are, depending on the distance from the observer, up to 60 2dFGRS groups and field galaxies outside groups.

The multiplicity of Abell superclusters was derived by Einasto et al. (1994). The distribution of multiplicities is rather close to the distribution found in the present paper. The multiplicity of simulated superclusters was studied by Wray et al. using rich DM-halos. The multiplicity function was derived for a number of linking lengths. The linking length $L = 5\ h^{-1}$ Mpc corresponds approximately to our accepted threshold density. The integrated multiplicity function is presented in their Fig. 3. The case $L = 5\ h^{-1}$ Mpc is rather similar to the multiplicity function of our DF-clusters. We shall discuss the multiplicity function and its cosmological consequences in separate papers by Saar et al (2006) and Einasto et al. (2006b).

A natural division of superclusters into poor, medium and rich systems would be according to the total luminosity.

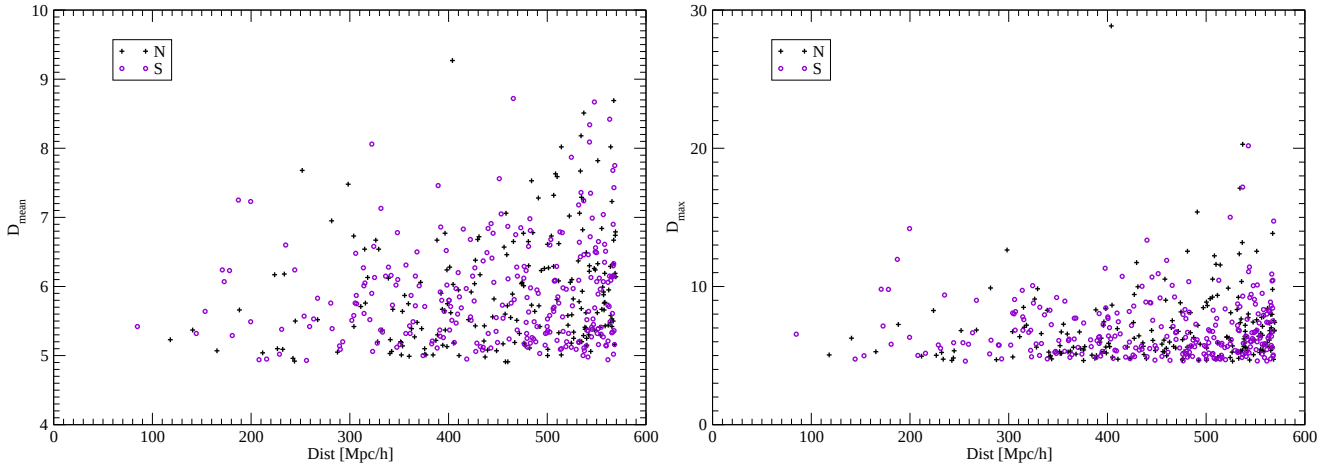

Fig. 2. The mean (left panel) and the maximal density (right panel) of superclusters at various distances from the observer.

However, it is not always easy to determine the total luminosity of superclusters. Another possibility to characterize the richness of superclusters is the number of high-density peaks, in our case DF-clusters. As we have seen above, the number of galaxies and groups is not suited for this purpose since both these numbers are influenced by selection effects. The number of DF-clusters is proportional to the supercluster total luminosity: the relationship is linear in the log-log diagram. Multiplicity of superclusters is easily determined from observation, also for superclusters found using Abell clusters or DM-halos in simulations.

We shall use the supercluster multiplicity to divide superclusters into four richness classes. We call superclusters which have less than 3 DF-clusters poor, superclusters with 3 to 9 DF-clusters medium rich, superclusters with 10 to 19 DF-clusters rich, and with 20 or more DF-clusters extremely rich superclusters. As shown above, DF-clusters are of the Abell class. As a prototype of a poor supercluster we can use the Virgo or Coma Supercluster, containing one and two Abell class clusters, respectively. A characteristic supercluster of medium richness class is the Perseus-Pisces Supercluster; its visible part contains 3 Abell clusters, but part of the supercluster is hidden in the zone of avoidance. Examples of nearby rich superclusters are the Leo-Sextans and Horologium-Reticulum Superclusters, and also the supercluster SCL126 (see Fig. 13 below). To the class of extremely rich superclusters belongs the Shapley Supercluster.

We have used these richness classes and determined for all richness classes median values of various parameters, determined in Paper I for 2dFGRS superclusters. To get an idea of the spread in these parameters we calculated also the 1st and 4nd quantile of the distribution. Data are given in Table 1, both for the 2dFGRS and Millennium Simulation (sample Mill.F8) superclusters. Here N is the number of superclusters of the respective richness class, denoted by P, M, R and E for poor, medium, rich, and extremely rich superclusters, respectively (the numbers are given only once, they are identical for all quantities given in the Table). The quantities are: the luminosity L_{tot} (in Solar units); the absolute magnitude of the main galaxy M_m (in the b_j filter passband for 2dFGRS, and in the g filter passband for the Millennium Simulation); the mean and maximal densities, δ_m and δ_p, respectively (in units of the mean density); the maximal diameter D_{max} (diagonal of the rectangular box around the supercluster) and the effective diameter D_e (the diameter of the sphere equal in volume to that of the supercluster, both in h^{-1} Mpc); the center offset parameter Δ_o (the distance between the geometric and dynamic center, also in h^{-1} Mpc); and the ratio of the effective to the mean diameter ϵ_0.

The number of DF-clusters in superclusters is on average the same in nearby and distant superclusters (see Fig. 1). There is a strong dependence of the number of DF-clusters with the total luminosity of superclusters. A look at Table 1 shows that about 2/3 of the superclusters are poor, both in the real and simulated samples – i.e. they belong to the same supercluster richness class as the Local and Coma Superclusters. With increasing total luminosity the number of DF-clusters – or the multiplicity of superclusters – increases.

However, there exists a remarkable difference between the distribution of supercluster richness classes for the real and simulated samples. For the 2dFGRS supercluster sample, 5% of the superclusters are of richness class R and E, and the richest superclusters have up to about 60 DF-clusters. In contrast, only 1% of the Millennium Simulation supercluster sample has this richness class, and the richest simulated superclusters have only 20 DF-clusters. This difference in the richness of real and simulated superclusters is one of the major results of our study. A further discussion of this problem is given by Saar et al. (2006).

4. Properties of real and simulated superclusters

4.1. Supercluster properties as a function of distance

The major problem in using flux-limited galaxy samples is the magnitude selection effect. Faint galaxies and groups are not seen at large distances, thus it is expected that the number of visible galaxies and groups in superclusters decreases with distance. This is what is actually observed: there exists a lower limit of the number of galaxies and groups in superclusters, and this limit decreases with distance exponentially (Fig. 1). This

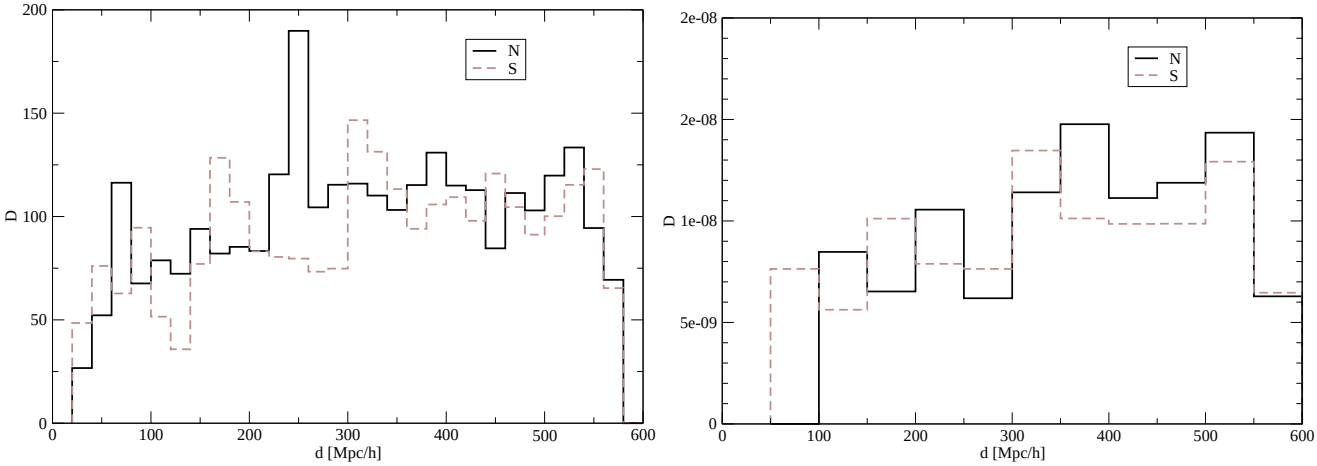

Fig. 3. Left panel: the mean luminosity density in the Northern and Southern regions of the 2dF as a function of distance. Right panel: the mean number density of 2dF superclusters as functions of distance.

selection effect distorts the number of galaxies and groups as supercluster richness indicators. For this reason we have used as richness indicator the number of local high-density peaks – DF-clusters (see right panel of Fig. 1). DF-clusters have been found using luminosities of galaxies and groups corrected for the effect of luminosity bias. (See Paper I for details of the reconstruction of estimated true total luminosities of DF-clusters and superclusters.) The right panel of Fig. 1 shows that the number of DF-clusters in superclusters – the supercluster multiplicity – is in the mean the same in nearby and distant superclusters. Due to the volume-effect there are no very rich superclusters at small distance $D < 300\ h^{-1}$ Mpc.

In Fig. 2 we show the mean and maximal luminosity density of superclusters at various distances from the observer, for the Northern and Southern regions. We see that the distributions are rather uniform – both densities are distributed similarly irrespective of distance.

The left panel of Fig. 3 shows the mean luminosity density of the whole 2dFGRS sample, separately for the Northern and Southern regions. There are several peaks due to very rich superclusters, but in general the luminosity density is approximately constant. The mean number density of superclusters is shown in the right panel of Fig. 3; it is also approximately the same at various distances from the observer. 2dFGRS samples are wedges and are rather thin at small distance from the observer. In such thin regions the identification of superclusters is problematic and hence the spatial density of superclusters at small distances is rather low. This is the only known distance-dependent selection effect in the supercluster sample.

4.2. Luminosities of superclusters

One of the major goals of the present study was the compilation of a representative sample of superclusters over a broad range of luminosities. This gives us the possibility to derive the luminosity function of superclusters. Results of our calculations are shown in Fig. 4. Our dataset is large enough to measure the luminosity function spanning almost 3 orders in luminosity and spatial density.

We have calculated the supercluster luminosity function separately for the main supercluster sample, which contains superclusters with distances up to 520 h^{-1} Mpc, and for the supplementary sample, containing more distant superclusters. In both cases Northern and Southern subsamples were stacked. The main samples have 379 superclusters, the supplementary ones 164. Our analysis has shown that the largest and most luminous superclusters have extensions beyond the boundaries of 2dFGRS. Thus the total luminosities of most luminous superclusters (SCL9 and SCL126 from the list by Einasto et al. (1997)) are probably underestimated.

Figure 4 shows that there are no large differences between luminosity functions found for the main and supplementary samples, only the scatter of the function of the supplementary sample is larger. This is due to two factors: the expected total luminosities of groups have random errors due to large weight factors used in the restoration of the expected total luminosities, and there are errors in the density field due to inaccuracies in the expected total luminosities. Due to the second error some superclusters fall below the threshold density and are missed, and some poor superclusters are added to our list which actually are fainter than our threshold density limit. In the mean these errors cancel each other out and increase only the scatter or supercluster luminosities. There is also a certain systematic trend: the supplementary list contains, in comparison to the main list, richer superclusters.

In Paper I we have compared luminosities of simulated superclusters calculated from the true density field and from the density field of simulated flux limited galaxy samples. This comparison has shown that luminosities of superclusters found from a flux limited sample are systematically fainter than 'true' luminosities found from all data. A detailed analysis is needed to investigate this and other biasing factors (including a detailed study of the structure of individual rich superclusters) to have a more accurate estimate of the supercluster luminosity function.

For comparison we show in the right panel of Fig. 4 the luminosity function of simulated superclusters extracted from the Millennium Simulation. The luminosity function was constructed in two ways. The solid line corresponds to the sam-

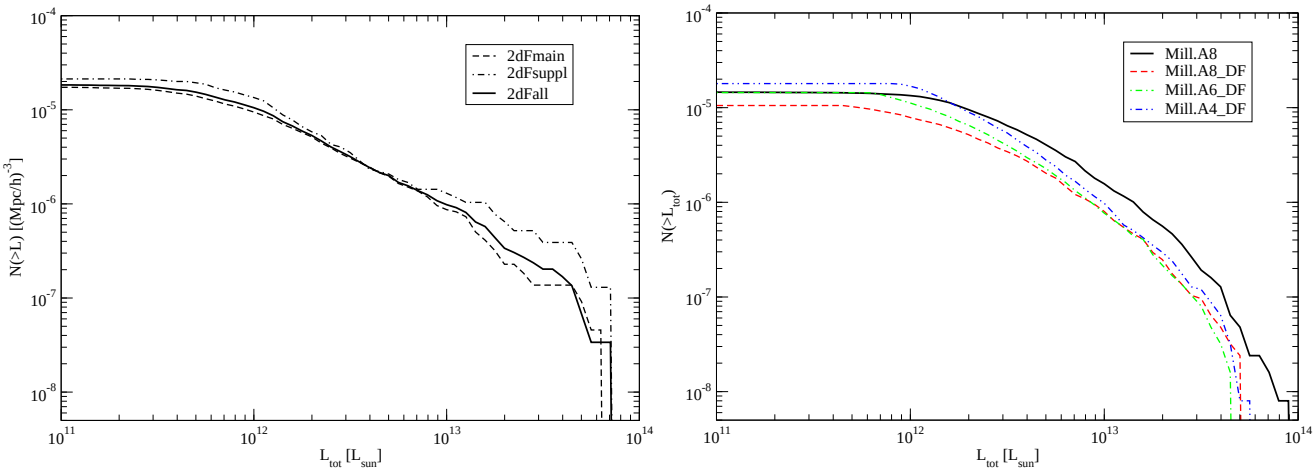

Fig. 4. The luminosity functions of superclusters. Left: 2dF superclusters, right: Millennium Simulation superclusters. The supercluster luminosity function for the 2dFGRS was calculated for the main, supplementary, and the total supercluster samples (North and South added), plotted with dashed, dot-dashed and solid curve, respectively. For simulated superclusters the solid bold curve is the luminosity function calculated by adding luminosities of supercluster member galaxies; dashed, dot-dashed and dot-dot-dashed curves correspond to Millennium samples Mill.A8, Mill.A6 and Mill.A4, in these cases the luminosity of superclusters was found from the density field.

ple Mill.A8 where luminosities of superclusters were found by adding luminosities of galaxies in superclusters. The supercluster sample includes systems with a minimal volume limit of 100 Mpc$^3h^{-3}$. Dashed, dot-dashed and dot-dot-dashed curves were calculated for models Mill.A8, Mill.A6 and Mill.A4, respectively, by integrating the luminosity density field inside the contour of the supercluster, multiplied by the mean luminosity per cell. Supercluster samples Mill.A8, Mill.A6, and Mill.A4 were found using Epanechnikov kernel with radius 8, 6, and 4 h^{-1} Mpc, respectively, see Paper I for details. In these models the limiting volume was taken to be 200 Mpc$^3h^{-3}$. We see that there exists a shift in luminosities between the two sets of data. This shift can be explained by the fact that, in the luminosity density field, part of the luminosity of galaxies is smoothed away beyond the threshold contour (see Fig. 13). For this reason total luminosities obtained from the density field are underestimates. To avoid this systematic bias we have used in the calculation of total luminosities of superclusters estimates based upon luminosities of supercluster member galaxies and galaxy groups/clusters.

The comparison of luminosity functions of the samples Mill.A8, Mill.A6, and Mill.A4 shows the effect of using different smoothing lengths in the calculation of the density field. The smaller the smoothing length, the more often outlying parts of superclusters have a tendency to form independent poor superclusters. This increases the number of poor superclusters and changes the resulting luminosity function. The figure shows that these changes are rather modest; in the range of high luminosities the frequency of superclusters of various luminosity is almost constant. If we use identical smoothing lengths and selection parameters (threshold density and lower volume limit) for models and real data, we get comparable supercluster samples.

The mean number-density of superclusters as defined in the present analysis is well determined: both the Northern and Southern regions of 2dF yield about 17 superclusters per million Mpc$^3h^{-3}$. A sample with similar selection parameters for the Millennium Simulation contains 14 superclusters per million Mpc$^3h^{-3}$ – i.e. the number densities of real and simulated superclusters are very similar. The number density of rich and extremely rich superclusters is much lower – 0.6 and 0.3 per million Mpc$^3h^{-3}$, respectively, in the real sample. If this density is characteristic for the whole Universe, then we have a chance to observe one extremely rich supercluster in a volume of 3 million Mpc$^3h^{-3}$. We note that nearby examples of rich and extremely rich superclusters SCL126 and SCL9 have actually a higher total luminosity than found in the 2dFGRS, since both are cut by the observational limits of the survey in declination, as seen from the density field. Larger deep galaxy redshift surveys are needed to find more accurate values of luminosities of these very rich superclusters.

The comparison of luminosity functions of real and simulated superclusters shows several differences. First, as noted above, the number density of rich and extremely rich superclusters in the simulated sample is much lower, only 0.15 per million Mpc$^3h^{-3}$. The other difference between total luminosities of real and simulated superclusters is in their median luminosity values. Table 1 shows that median luminosities of simulated superclusters of all richness classes are higher than median values of luminosities of 2dF superclusters by a factor of $2-4$. A similar shift is seen in the luminosity functions of the 2dF and Millennium Simulation galaxies. The reason of this discrepancy is not clear.

The third difference between luminosity functions of real and simulated superclusters is in the shape of the functions: the luminosity function of 2dFGRS superclusters has an almost constant slope in the $\log L_{tot}$ vs. $\log N(> L_{tot})$ diagram, whereas the luminosity function of simulated superclusters has a continuous change of the slope.

The general shape of the integrated luminosity function, found here for the 2dFGRS and Millennium Simulation supercluster samples, is rather close to the theoretical luminos-

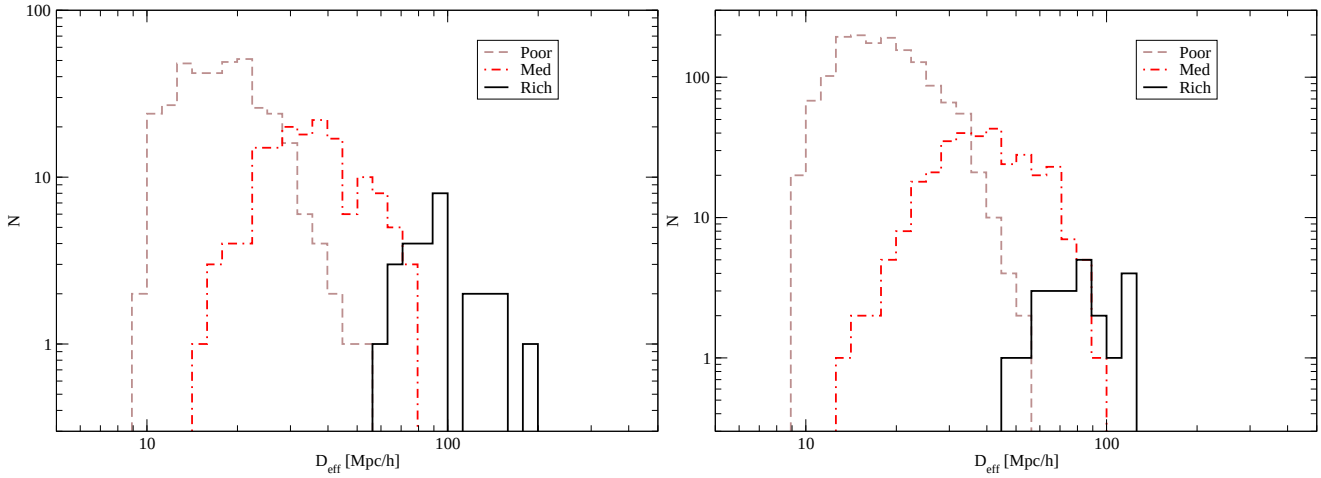

Fig. 5. The distribution of maximal diameters of poor, medium, and rich superclusters, defined by supercluster multiplicity. Left panel shows data for 2dFGRS superclusters (Northern and Southern regions together), right panel Mill.A8 superclusters.

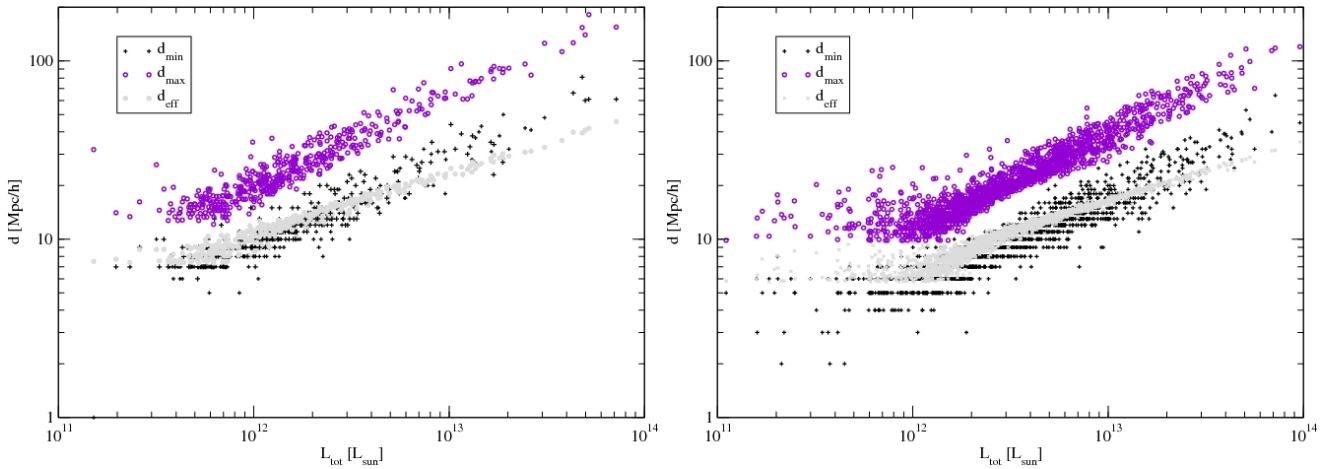

Fig. 6. The minimal, maximal and effective diameter of superclusters of various total luminosity. The left panel shows data for 2dF superclusters, the right panel for Millennium Simulation superclusters.

ity function calculated by Oguri et al. (2004) using the Press-Schechter approximation. Both real and simulated supercluster samples span an interval of total luminosities exceeding two orders of magnitude, similar to the range of luminosities discussed by Oguri et al. They compared the model with the sample of superclusters of SDSS by E03a, which was compiled on the basis of the 2-dimensional density field. This sample covered only one decade in total luminosity. The present paper gives improved possibilities for comparison. Also, the number of DF-clusters found in the present analysis is close to the number of clusters in simulations by Oguri et al.

4.3. Sizes of superclusters

Next we study the geometric properties of DF superclusters. As an argument we use the total luminosity of superclusters which was found by summing all estimated total luminosities of member galaxies and groups/clusters in the supercluster. As geometric quantities we consider the minimal diameter (along one of the coordinate axes, whatever is the smallest), the maximal diameter of the supercluster defined as the length of the diagonal of the rectangular box surrounding the supercluster along coordinate axes, and the effective diameter – the diameter of the sphere equal to the volume of the supercluster (remember that the volume is defined as the number of cells which have a density equal or greater than the threshold density, where the cell size is 1 $(h^{-1}\,\mathrm{Mpc})^3$).

The distribution of the maximal diameters of poor, medium, and rich superclusters is shown in Fig. 5 for the 2dFGRS and Millennium Simulation superclusters, median values and quantiles for superclusters of different richness class are given in Table 1. As expected, the maximal diameters depend strongly on the supercluster richness, both in the real data and in the simulations. Median values of maximal (and minimal) diameters of superclusters of various richness are in good agreement with semiaxis lengths for Abell superclusters (Jaaniste et al. 1998) and LCRS superclusters (Doroshkevich et al. 2001) of similar richness. An even closer correlation exists between the effective diameter and the total luminosity, shown in Fig. 6. The scatter in this relationship is the smallest and the relationship in log-log representation is linear.

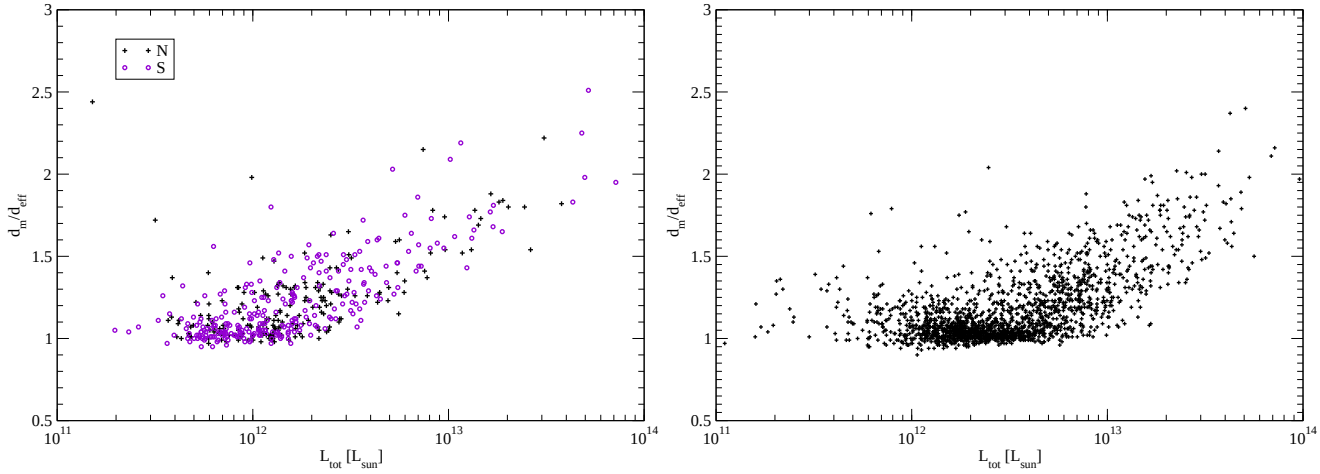

Fig. 7. The ratio of the mean diameter to the effective diameter in superclusters of various total luminosity. The left panel shows data for 2dF superclusters, the right panel for Millennium Simulation superclusters.

Figure 6 demonstrates one important aspect of our supercluster catalogue: the total luminosities and sizes of superclusters have a rather sharp lower limit. This limit is determined by two selection parameters: the density threshold and the volume threshold. The density threshold excludes systems of galaxies of low density from the sample, and the volume threshold excludes small systems like single clusters. We have used values as low as possible in our supercluster selection in an attempt to include all galaxy systems which could be classified as superclusters. The analysis presented above has shown that the choice of these selection parameters has been rather successful: the sample of superclusters is fairly homogeneous. With our choice of selection parameters we have excluded about 60% of galaxies. As noted above, these galaxies are located in less dense galaxy systems, and the main galaxies of these poor systems have a much broader distribution of luminosities and their mean luminosities are also considerably lower (see Paper III for more details). All this confirms that we have selected a practically complete sample of galaxy systems (within the observed region) which can be called superclusters.

4.4. Symmetry and compactness of superclusters

The axis ratios of superclusters have a mean value around unity in all three directions. More interesting is the dependence of the minimal, maximal and effective diameters on the expected total luminosity of the supercluster, shown in Fig. 6. This Figure shows that all three diameters are the larger the higher the total luminosity of the supercluster and the richer the supercluster (see Table 1). The dependence is, however, different for various diameters: the maximal diameter shows the fastest growth with luminosity, and the effective diameter the slowest growth. This difference is due to a variation of the shape and compactness of superclusters with differing luminosity.

The right panel of Fig. 6 shows the same set of axis ratios for superclusters found in the Millennium Simulation Mill.F8. The general trend is very close to the trend seen in the real supercluster sample. This similarity shows that geometric properties of simulated superclusters fit real data very well.

The ratio of the mean diameter (the average of the extensions along 3-coordinate axes) to the effective diameter is plotted in Fig. 7, in the left panel for 2dFGRS superclusters, and in the right panel for Millennium Simulation superclusters. This ratio depends on the compactness and the filling factor of the system. The ratio is the larger the more empty space (more accurately, regions of space of luminosity density below the threshold density) is located in the vicinity of the system defined by galaxy filaments belonging to the system. The Figure shows that in poor superclusters this ratio is close to unity (the minimum by definition). In other words, poor superclusters are rather compact systems. Here a good example is the Local Supercluster, which contains only one rich cluster, the Virgo cluster, close to its center, and is surrounded by numerous galaxy filaments. These filaments have low luminosity density and fall outside the threshold density. Thus systems like the Local supercluster are in our catalogue presented only by their cores, which are compact and rather spherical, due to the symmetrical smoothing of the density field. The actual shape of compact superclusters can be investigated using the distribution galaxies or groups (see the next subsection).

The scatter of values about unity for poor superclusters is partly due to errors of the mean diameter. Supercluster sizes have been found from density field cells with extreme values of coordinates inside the threshold contour, they can only be determined with an accuracy of $\pm 1\ h^{-1}$ Mpc. The mean diameters of smallest systems are of the order of $10\ h^{-1}$ Mpc, thus a relative error of about 10% is expected for the ratio of diameters of small systems. In almost all rich superclusters the mean diameter is much higher than the effective diameter, i.e. these systems have a lower compactness and filling factor. This result agrees with that in E97, in which we showed that rich superclusters have smaller fractal dimensions and are more filament-like than poor superclusters.

Figure 8 shows the offset of the geometrical center from the dynamical one, again for the 2dFGRS and Millennium Simulation superclusters. The center offset parameter was defined as follows: $\Delta_o = ((x_0 - x_m)^2 + (y_0 - y_m)^2 + (z_0 - z_m)^2)^{1/2}$; here x_0, y_0, z_0 are coordinates of the geometric center of the su-

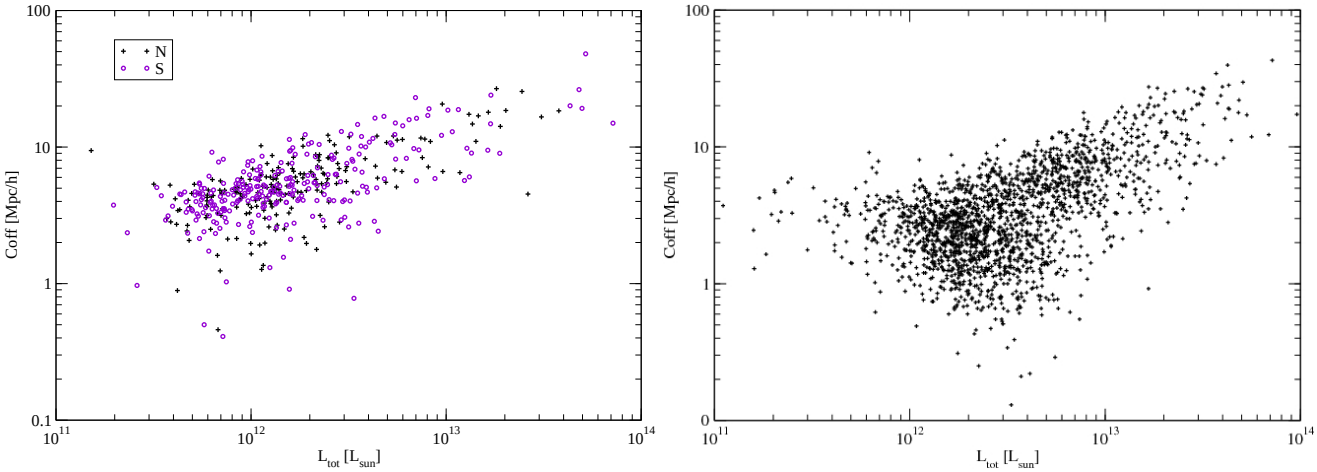

Fig. 8. The offset of the geometrical center from the dynamical one as a function of the total estimated luminosity of superclusters. Left panel shows 2dF superclusters, right panel Millennium Simulation superclusters.

percluster, found on the basis of extreme values of coordinates of the rectangular box containing the system, and x_m, y_m, z_m are coordinates of the dynamical center of the supercluster, defined by the main cluster of the supercluster. In the ideal case it would be better to determine the dynamical center using the gravitational potential field. We have used instead the center of the most luminous cluster near the highest density peak of the system. Poor and medium superclusters have relatively small offset of up to 10 h^{-1} Mpc, but the offset of very rich superclusters can reach values of up to 50 h^{-1} Mpc. In other words, poor superclusters are fairly symmetrical, but luminous superclusters are asymmetric: the system of filaments has different lengths in various directions. Actually filaments form a continuous web, only in some parts the density of galaxies in filaments is lower and falls below the threshold used to compile galaxy systems. The Figure also shows that there are no sharp boundaries between superclusters of low and high luminosity – i.e., the transition is smooth.

4.5. The shape of superclusters

To study the shape of superclusters we approximate the spatial distribution of galaxies or groups in superclusters by a 3-dimensional mass ellipsoid and determine its centre, volume and principal axes. In most cases our superclusters do not form a regular body; however, these parameters can be used as a first approximation to describe the density and alignments of the elements of large-scale structure.

In the present study we use the classical mass ellipsoid (see e.g. Korn & Korn 1961):

$$\sum_{i,j=1}^{3} \left(\lambda_{ij}\right)^{-1} x_i x_j = 5, \qquad (1)$$

where

$$\lambda_{ij} = \frac{1}{N_{gr}} \sum_{l=1}^{N_{gr}} (x_i^l - \xi_i)(x_j^l - \xi_j), \qquad (2)$$

is the inertia tensor for equally weighted groups, N_{gr} is the total number of groups, and $\xi_i = \frac{1}{N_{gr}} \sum_{l=1}^{N_{gr}} x_i^l$ determines the Cartesian coordinates of the centre of mass of the system.

The formula determines a 3-dimensional ellipsoidal surface with the distance from the centre of the ellipsoid equal to the rms deviation of individual objects in the corresponding direction. This method can be applied for superclusters with $N_{gr} \geq 5$. The problems related to the stability of the method and the influence of observational errors have been discussed in Jaaniste et al. (1998).

To investigate the sensitivity of the method to the number of groups we divided our sample of mass ellipsoids into three richness classes, Xrich with the number of groups $N_{gr} \geq 100$, Xmed with $100 > N_{gr} \geq 10$, and Xpoor with $N_{gr} < 10$; here X denotes N for the 2dFGRS Northern sample and S the Southern one. Superclusters with the number of groups exceeding 10 are more-or-less uniformly distributed in distance, whereas poor superclusters are all located at distance exceeding 300 h^{-1} Mpc (see also Fig. 1). In Figure 9 we show in the left panel the semi-minor axis a and the semi-major axis c as a function of the supercluster total luminosity. We see that poor superclusters have a large scatter of semi-axis length values. In particular, the length of the semi-minor axis is for some superclusters less than 1 h^{-1} Mpc. As all these superclusters are distant objects with only a few groups/clusters in the visibility window, we assume that this large scatter is due to small number of objects. Nearby superclusters of similar total luminosity have considerably larger values of the semi-minor axis a and a much smaller scatter. To avoid this uncertainty we exclude samples of poor superclusters with $N_{gr} < 10$ from the further analysis.

Fig. 9 right panel shows the bivariate distribution of axial ratios a/b vs. b/c. This figure can be compared directly with Figures 9 - 11 of Wray et al. (2006) for samples of simulated superclusters. Wray et al. defined superclusters as clusters of rich DM-clusters. They used several linking lengths to compile supercluster catalogues. The largest linking length yields percolating superclusters and cannot be compared with our results, but the linking length $L = 5\ h^{-1}$ Mpc corresponds approximately to our accepted threshold density (Fig. 11 of Wray

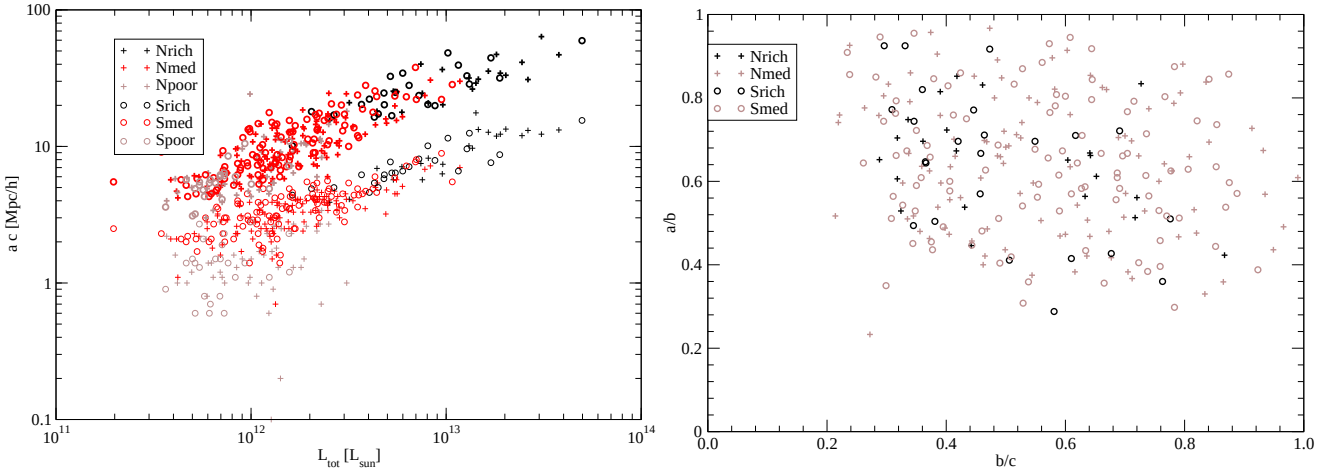

Fig. 9. Left panel: the semi-minor and semi-major axes of the mass ellipsoid, a and c, are plotted for superclusters of different total luminosities. Bold symbols are for the semi-major axis, and thin ones for the semi-minor axis. Superclusters of various richness are shown with different symbols. Right panel: axial ratios of superclusters a/b vs. b/c for superclusters with at least 10 member groups. Filamentary superclusters populate the upper left part of the figure, spherical superclusters the upper right part, and pancake-like structures the lower right section. Triaxial superclusters are located in the central region.

et al.). The comparison of our Figure 9 with the corresponding figure by Wray et al. shows very good agreement. Both distributions show that there are no purely filamentary, spherical or pancake-like superclusters: almost all superclusters are triaxial, with some tendency toward filamentary character.

We further note that Figure 9 is akin to Figure 6. Whereas the former shows the length of the semi-minor and semi-major axes a and c for superclusters of various total luminosities, the latter presents minimal, maximal, and effective diameters of superclusters found from the density field. Semi-axes of the mass ellipsoid are about one-half to one-third the size of their respective diameters, as would be expected.

This analysis complements our previous analysis based on the density field. One small remark should be added: if the supercluster only barely meets our threshold density criterion, and only its tip exceeds the threshold density level, then, by definition, the density field above the threshold is almost spherical in shape, due to the symmetrical smoothing law applied in the determination of the density field. Thus the true shape of poor superclusters cannot be determined from the density field alone. Here the distribution of objects within the supercluster can help, but only, if the number of objects exceeds 10.

A similar conclusion on the shape of superclusters has been reached by Jaaniste et al. (1998). Basilakos et al. (2001) and Basilakos (2003) applied shape-finders introduced by Sahni et al. (1998), to find the shape characteristics of PSCz and SDSS superclusters. PSCz superclusters were defined by the density field method using rather large cell sizes of 5 and 10 h^{-1} Mpc. SDSS superclusters were found on the basis of Cut and Enhance clusters by Goto et al. (2002). In both cases this statistic suggests that filaments dominate over pancakes. Kolokotronis et al. (2002) compared shapes of Abell superclusters with simulated superclusters using the same shape-finder statistics. Again a dominance of filamentary structures both in real and simulated superclusters was found. Doroshkevich et al. (2001) determined effective dimension for galaxy systems in high- and low-density regions, which correspond to our supercluster and field samples. For the supercluster sample they found the dimension 1.6 ± 0.2, and for the field sample 1.0 ± 0.17, which correspond to sheets and filaments, respectively. Klypin et al. (1989) investigated fractal dimensions of nearby superclusters (Virgo, Coma) and galaxy filaments surrounding them. For superclusters they found effective dimensions 1.8 - 2.0, for inter-supercluster regions 1.3.

An inspection of the density fields of 2dFGRS samples shows that actually the shape of rich superclusters is more complicated. It cannot be presented by a simple ellipsoid. The density field shows that most superclusters are multi-branched, i.e. they consists of numerous density knots arranged along several cluster chains. This morphology was detected already in the Perseus-Pisces supercluster by Jõeveer et al. (1978), Einasto et al. (1980) and Zeldovich et al. (1982).

4.6. Densities of superclusters

The mean luminosity density in superclusters is presented in Fig. 10 for 2dFGRS samples and for the Millennium Simulation sample. The mean density rises from 4.5 for poor to 6 – 10 for rich superclusters. We see also a gradual increase of the mean density with increasing total luminosity. This fact is very important, since it demonstrates that rich superclusters are dense systems, not just percolations of several loose systems.

The maximal luminosity density of superclusters (the smoothed density near the dynamical center) is shown in Fig. 11. Here the trend with supercluster total luminosity is even more pronounced: very luminous superclusters have also high-density peaks at their centers. The maximal density increases from 5 in poor superclusters to about 20 in rich ones. Note that the maximal density of poor superclusters in many cases only marginally exceeds the mean density (about 5), and both are very close to the threshold density 4.6 used in the com-

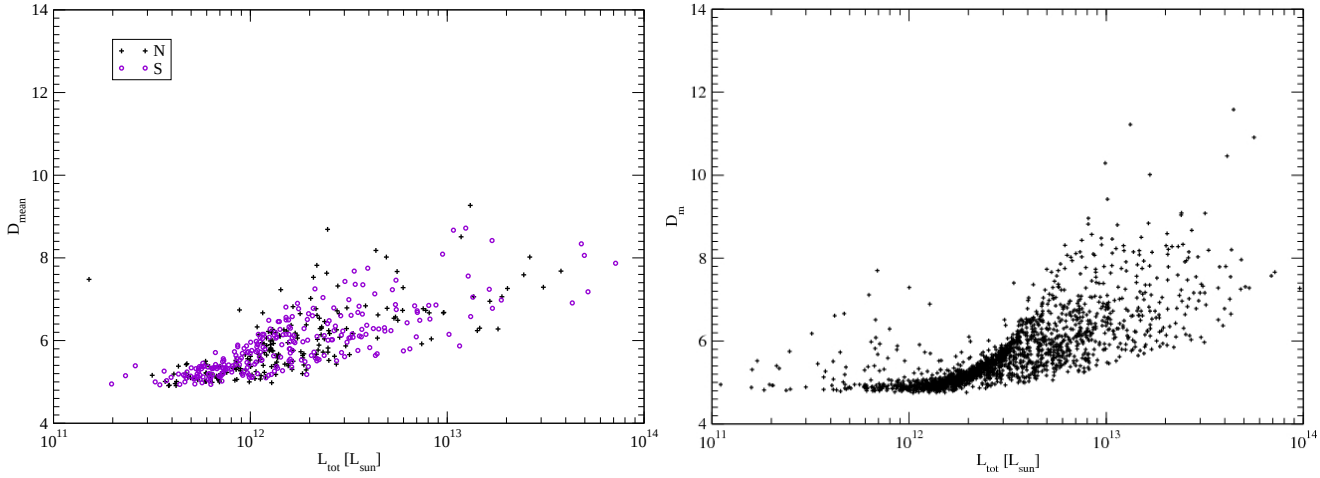

Fig. 10. Mean density of superclusters as functions of the total luminosity of the supercluster. Left panel shows data for 2dF samples, right panel for Millennium Simulation data, calculated with minimal volume 100 $(h^{-1}\,\mathrm{Mpc})^3$.

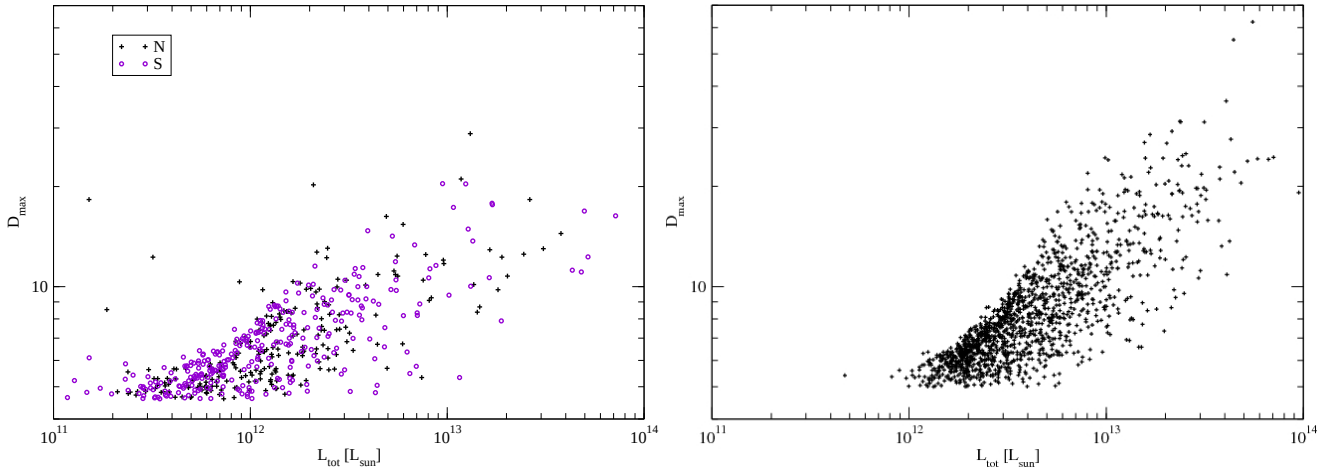

Fig. 11. Maximal density of superclusters as functions of the total luminosity of the supercluster. Left panel shows data for 2dFGRS samples, right panel for Millennium Simulation data, calculated with minimal volume 200 $(h^{-1}\,\mathrm{Mpc})^3$. Notice the difference in the number of poor superclusters.

pilation of the supercluster catalogues. This demonstrates that poor superclusters are small density enhancements with a low scatter of internal density.

Note, however, that the supercluster with the highest luminosity has not the highest mean and maximal density, but a bit lower than the highest values. This is the case both for the real as well as the simulated supercluster sample. This indicates that these largest superclusters are not the very densest, but consist of a number of subunits of slightly lower mean and maximal density.

5. Discussion

5.1. Possible biases and errors of supercluster parameters

There are two types of errors in our supercluster catalogue. Systematic errors are due to uncertainties in the selection algorithms and in the input parameters in the selection of superclusters. Random errors are due to observational errors and errors due to the small numbers of observed galaxies in superclusters.

Random errors in the galaxy positions are negligible. More serious are errors in redshifts and in magnitudes. Large errors in redshift are very seldom and move the galaxy completely outside the supercluster in question, thus these errors influence the number of galaxies in the system. Ordinary redshift errors increase the redshift scatter of galaxies in groups and single galaxies inside superclusters. The scatter inside groups is taken into account during the group selection procedure. In this paper we have used the mean redshifts of galaxies in groups. The influence of random errors on the mean redshift of groups is small, in most cases less than 1 h^{-1} Mpc (if the redshift error is transformed to distance error). Redshift errors of single galaxies are larger, but also do not exceed considerably 1 h^{-1} Mpc, the size of an elementary cell in the density field. Since densities are smoothed with an Epanechnikov kernel of radius 8 h^{-1} Mpc, these errors do not influence our results.

Errors in magnitudes, in particular the corrections due to unobserved galaxies, are the most serious random errors in our supercluster catalogue. These errors increase the scatter of expected total luminosities of superclusters. More important are

the errors of the density field due to the use of corrected expected luminosities of galaxies. As suggested by Basilakos et al. (2001), the smoothing of the density field may introduce a systematic error which increases densities above the mean density and decreases densities below the mean (see their Fig. 1). To investigate how serious this error is in our case, we compared two density fields of the Millennium Simulation, Mill.A8 and Mill.F8, and calculated the quantity

$$\Delta(r) = \frac{\rho_F(r) - \rho_A(r)}{\rho_A(r)}, \quad (3)$$

where $\rho_A(r)$ is the mean density found for the original sample Mill.A8, and $\rho_F(r)$ is the mean density found for the simulated 2dF sample. Mean values were found for a series of distance intervals from the observer. The results of the calculation are shown in Fig. 12. The trend is the same as found by Basilakos et al., but the errors are about 10 times smaller. This difference in errors is probably due to the use of very different cell sizes: in our case the size was 1 h^{-1} Mpc, whereas Basilakos et al. used cell sizes 5 and 10 h^{-1} Mpc. In other words, deriving the density field using a small cell size and calculating from flux-limited galaxy data does not introduce noticeable systematic errors. Random errors in the density field are larger, as seen from the comparison of supercluster total luminosities found for samples Mill.A8 and Mill.F8 (see Paper I).

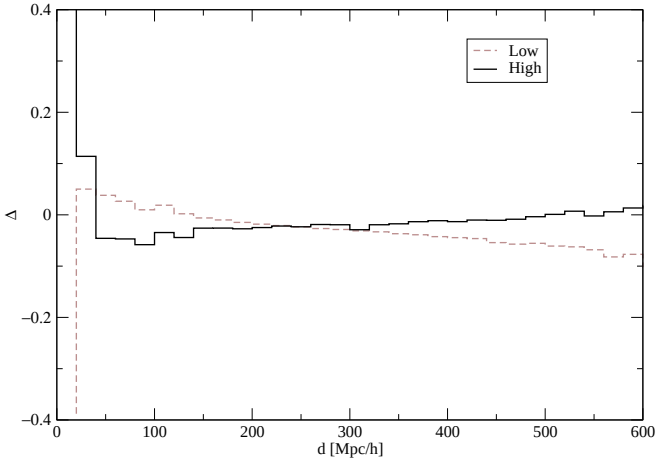

Fig. 12. The mean difference of the density between density fields of Mill.A8 and Mill.F8, at various distances from the 'observer'. The solid line shows differences in overdensity regions, the dashed line in under-density regions.

The most serious errors in our catalogue are due to the small number of galaxies observed in distant superclusters. As seen from Figure 1, the number of galaxies observed in superclusters has a lower limit which decreases with increasing distance according to the same law as found by shifting groups of galaxies to larger distance (see T06). At the outer limit of our galaxy sample at $z = 0.2$ the lower limit of the number of galaxies observed in superclusters approaches $N_{gal} = 1$. It is clear that one galaxy is not sufficient to define a supercluster, even a poor one. Thus we have excluded superclusters with a number of groups below 3 from our list. Furthermore, the catalogue was divided into two parts, the main catalogue A and the supplementary catalogue B. The main catalogue has systems up to distance 520 h^{-1} Mpc, and the supplementary one even more distant objects. We have found the luminosity function of superclusters separately for the main and the supplementary supercluster sample (see Fig. 4). The luminosity function of the supplementary sample has a larger scatter and lies higher for rich superclusters.

Table 2. Identification of rich 2dF Northern superclusters in another supercluster catalogues

ID	ID_W	ID_{ACO}	N_{cl}	N_{gr}	N_{ACO}	N_{2dF}	N_X	N
1	2	3	4	5	6	7	8	9
13	07	82	10	1145	4	11		
20	01	88	2	556	1	7	2	1.
37		265	9	359	1	2		
76	07,08	100	5	420	1	4		
77		91	2	315	1	3	1	2.
78			5	57	1	2		
82	08,11		3	187	1	10		
92	08	100,265	3	315	2,1	3,4		3.
97	08	265	5	129	2	5		
99			13	472	8	14		
108			24	169	1	2		
120			19	207	1	1		
136	14		2	251	1	2		
152	06	111,126	18	3591	2,7	2,40	5	4.
170	10		8	415				
205	12		5	215	1	2		
220			16	426	2	2		

Colums:
1 - 2dFGRS supercluster ID number,
2 - ID number by Erdogdu et al.,
3 - Abell supercluster ID number (E01),
4 - number of DF clusters,
5 - number of 2dFGRS groups + field galaxies,
6 - number of Abell clusters,
7 - number of 2dFGRS groups (T06),
8 - number of X-ray clusters,
9 - name (see Notes).
Notes: 1. Sextans; 2. Leo-Sextans; 3. Leo-A; 4.Virgo-Coma

5.2. Comparison with other supercluster catalogues

In Tables 2 and 3 we give the identification of superclusters from our lists with the list by Erdogdu et al. (2004) obtained using the Wiener Filter method, and with Abell superclusters by Einasto et al. (2001). For superclusters which have no partners in the Abell supercluster list, we give the number of Abell clusters within the volume of the supercluster. The reason for the absence of the supercluster in the Abell supercluster list can be either a too low number of Abell clusters in the supercluster volume (identified in Abell supercluster search as isolated Abell cluster), or the clusters was too distant to be included

Table 3. Identification of rich 2dF Southern superclusters in another supercluster catalogues

ID	ID_W	ID_{ACO}	N_{cl}	N_{gr}	N_{ACO}	N_{2dF}	N_X	N
1	2	3	4	5	6	7	8	9
5	04	10	5	952	1	5	5	1.
10			17	535	2	5		
11			3	101	1	1		
19			2	91	1	5		
34	16	5,9	24	3175	2,8	9,26	6	2.
51	18		7	272	1	3		
60			4	132	1	1		
78			20	254	1	1		
84			3	225	3	4		
87			4	166	4	8		
88			2	105	1	1		
94	18		15	245	1	2		
109	15	232	2	249	2	7		
115			10	265	1	2		
116		232	3	230	2	4		
126	15		3	291	2	8		
152			4	180	1	1		
148			11	328	4	9		
153	15		8	64	1	5		
167	06	49	2	771	2	2	1	
190			5	122	1	4		
200			6	155	1	1		
204		190	5	342	2	5		
217			42	938	4	12		
222		199	2	473	1	4		
240			6	171	3	6		
267			6	173	2	5		
276			8	371	1	2		
303			5	71	1	2		

Notes: 1. Pisces-Cetus, 2. Sculptor

in the Abell supercluster catalogue. The commonly used name given in the ninth columns is according to Abell supercluster catalogue by E01.

This comparison shows that there exist no one-to-one relationship between superclusters of our lists and the lists by other authors. Differences are due to the usage of different techniques in supercluster definition and to the usage of different observational data.

Erdogdu et al. used a much larger and variable cell size when deriving the smoothed density field, thus their method has lower resolution than ours. Taking this into account, it is not surprising that several superclusters found with the Wiener filtering method are split into separate systems in our list. For instance, the Wiener Northern supercluster 08 combines our superclusters 76, 82, 92 and 97, and the Wiener Southern superclusters 15 and 18 are combinations of our superclusters 109, 126 and 51, 94, respectively. If we use a lower threshold density, then at a certain level our method also joins these superclusters to single systems. We repeat that the actual web of superclusters and filaments is a continuous one, and it is matter of convention how to join parts of this web to particular systems.

Abell superclusters were found using only Abell clusters as tracers – no individual galaxy information was used. Also the linking length used to combine clusters into superclusters corresponds to a much lower threshold density in our method. Due to these differences in data and method, one would expect to see more differences in the results. Actually there exists a rather good correspondence between our and Abell superclusters. Most notable differences are that Abell supercluster 265 is divided in our list into three entries (37, 92 and 97) in the Northern region, and that Abell 232 is a combination of our 109 and 116 in the Southern region. But there are also examples in another direction: the most prominent supercluster in the Northern region, 152 in our list and 06 in the Wiener supercluster list, is partly divided into Abell superclusters 111 and 126.

5.3. Comparison of real and simulated superclusters

The comparison of properties of simulated superclusters with real superclusters shows that in most cases simulated superclusters have relations between various parameters and the total luminosity which are almost identical to similar relations for real superclusters. There are some differences: the luminosity and the multiplicity functions of the Millennium Simulation superclusters do not contain as many very rich superclusters as is found in the 2dFGRS sample. We shall discuss these differences in more detail elsewhere (Einasto et al. 2006b, Saar et al. 2006).

The similarity of results for real and simulated superclusters has several consequences. First of all, it shows that our procedures to define superclusters and their parameters are rather robust and yield stable results. Secondly, it shows that simulations have reached a stage which produces superclusters of galaxies with properties very close to the observations.

5.4. Superclusters and the cosmic web

Superclusters are large-scale density enhancements in the cosmic web, the supercluster-void network. Rich and very rich superclusters contain rich clusters of galaxies in a relatively small volume, thus such objects are easily detected. Their properties depend on the method of selection of superclusters, but the principal properties are fairly stable. As an example we show in Figure 13 the low- and high-resolution density fields through the richest supercluster in the 2dFGRS Northern region, SCL126. This supercluster has been called the Sloan Great Wall (Vogeley et al. 2004, Gott et al. 2005, Nichol et al. 2006). Actually, the wall-like shape is due to the enhancement of the structure, as at this distance the observed spatial density of galaxies in the flux limited 2dFGRS and SDSS samples has a maximum. Praton, Melott, & McKee (1997) refer to this as the "Bull's Eye" effect. We see that the density contour 4.6 includes only the main body of the supercluster, the outlying parts and galaxy filaments (seen in the high-resolution density field) remaining outside the supercluster volume. Similarly, in

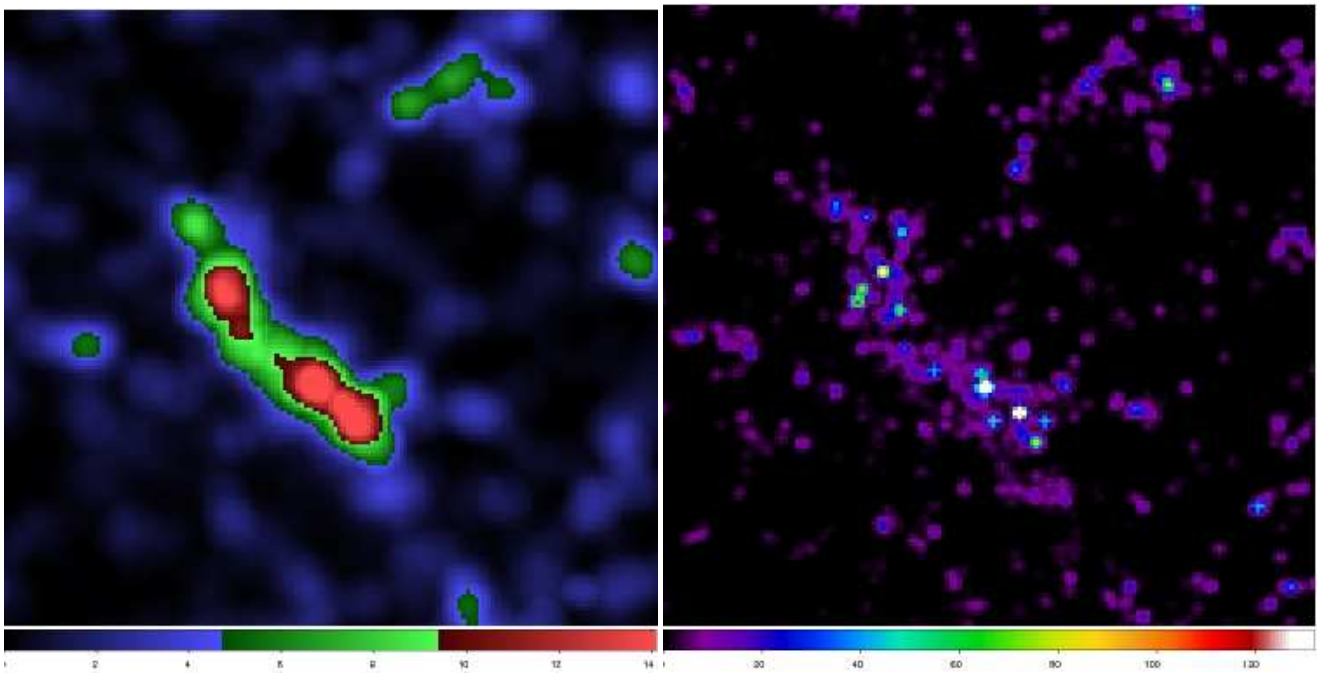

Fig. 13. The density field through the supercluster SCL126. Left panel shows the low-resolution field, the right panel the high-resolution field. In the low-resolution field the contour limiting green and blue regions corresponds to threshold density 4.6 in units of the mean density, which separates supercluster regions from low-density ones.

poor superclusters, the supercluster volume contains only the central core of the supercluster.

Very rich superclusters have been found also in our vicinity outside the 2dFGRS and SDSS surveys: the Shapley Supercluster and the Horologium-Reticulum Supercluster (see Proust et al. 2006, Fleenor et al. 2005 and Ragone et al. 2006 and references therein).

Most superclusters discussed in this paper are poor. They form small and medium density enhancements in the cosmic web. The web is a continuous network of filaments and sheets of galaxies, and there exist density enhancements of very different scale and luminosity. This continuous network of filaments was investigated recently by Sousbie et al. (2006). They found an algorithm which allows one to find the 3-dimensional filamentary skeleton of the equatorial slice of the SDSS. This slice is overlapped by the 2dFGRS Northern region and is centered around the supercluster SCL126, the Sloan Great Wall. The density field method with a certain threshold density allows one to identify as superclusters only their denser parts. As shown by Sousbie et al. and seen in Figure 13, the filamentary network continues outside superclusters.

There exist numerous investigations concerning the shape of structural elements of the cosmic web: Bond et al. (1996), Doroshkevich et al. (2001, 2004), Kasun & Evrard 2004, Shen et al. (2005), Sousbie et al. (2006), to name only a few studies. Doroshkevich et al. (2001) find that about 40 - 50 % of all galaxies belong to the "wall" (i.e. supercluster) population. This is in very good agreement with our results: we find that for threshold density 4.6 the fraction of galaxies in the supercluster population is 42 % (in both 2dFGRS regions). The volume filled with superclusters is much lower: 3.2 % in the Northern region, and 3.5 % in the Southern one. This volume filling factor is two times lower than found by E05b for simulated supercluster population. The difference my be explained by the use of lower threshold density by E05b (2.66 in units of the mean density).

6. Conclusions

We made an analysis of properties of superclusters listed in Paper I. Properties of real superclusters have been compared with properties of simulated superclusters from the Millennium Simulation, using identical procedures to collect galaxies to superclusters.

- We find that our sample of superclusters forms a homogeneous sample of galaxy systems, where properties of superclusters smoothly change with the total luminosity and multiplicity of the supercluster. Using the multiplicity we divide superclusters into four richness classes: poor, medium, rich and extremely rich.
- We investigated the shape of superclusters using groups of galaxies located inside superclusters, and the configuration of the density field above threshold used to define superclusters. We find that rich superclusters are more asymmetrical and have a smaller filling factor than poor ones. The asymmetry is characterized by the offset of the geometrical mean center from the dynamical one, defined as the center of the main cluster. Another manifestation of the asymmetry is the ratio of the mean diameter to the effective diameter (the diameter of a sphere equal to the volume of the supercluster); this ratio characterizes the filling factor and the degree of filamentarity of the system.
- We find that the mean and the maximal densities of superclusters increase when going from poor to rich superclus-

ters. This fact demonstrates that rich superclusters are not due to artificial percolation of poorer superclusters: they form a class of galaxy systems with properties continuously changing with supercluster richness.

– We calculated the luminosity and the multiplicity functions of superclusters; both span over two decades in luminosity and spatial density. The richest superclusters of the 2dFGRS sample contains up to 60 DF-clusters, whereas the the richest superclusters of simulated superclusters contains only up to 20. This is the main difference of simulated supercluster sample from observations.
– The comparison of properties of 2dFGRS superclusters with those of superclusters found for the Millennium Simulation shows that almost all geometric properties of simulated superclusters are very close to similar properties of real superclusters of the 2dFGRS sample.

Acknowledgements. We are pleased to thank the 2dFGRS Team for the publicly available final data release. The Millennium Simulation used in this paper was carried out by the Virgo Supercomputing Consortium at the Computing Centre of the Max-Planck Society in Garching. This research has made use of SAOImage DS9, developed by Smithsonian Astrophysical Observatory. The semi-analytic galaxy catalogue is publicly available at http://www.mpa-garching.mpg.de/galform/agnpaper. The present study was supported by Estonian Science Foundation grants No. 4695, 5347 and 6104 and 6106, and Estonian Ministry for Education and Science support by grant TO 0060058S98. This work has also been supported by the University of Valencia through a visiting professorship for Enn Saar and by the Spanish MCyT project AYA2003-08739-C02-01. D.T. was supported by the US Department of Energy under contract No. DE-AC02-76CH03000. J.E. thanks Astrophysikalisches Institut Potsdam (using DFG-grant 436 EST 17/2/05) for hospitality where part of this study was performed. In this paper we make use of R, a language for data analysis and graphics (Ihaka & Gentleman 1996).

References

Abell, G., 1958, ApJS 3, 211
Abell, G., Corwin, H., Olowin, R., 1989, ApJS 70, 1
Bahcall, N.A. 1988, ARA&A, 26, 631
Balogh, M., Eke, V., Miller, C. et al., 2004, MNRAS, 348, 1355
Basilakos, S., 2003, MNRAS, 344, 602 astro-ph/0302596
Basilakos, S., Plionis, M., Rowan-Robinson, M., 2001, MNRAS, 323, 47
Bond, J.R., Kofman, L., Pogosyan, D., 1996, Nature, 380, 603
Colless, M.M., Dalton, G.B., Maddox, S.J., et al. , 2001, MNRAS 328, 1039, (astro-ph/0106498)
Colless, M.M., Peterson, B.A., Jackson, C.A., et al. , 2003, (astro-ph/0306581)
Croton, D.J., Farra, G.R., Norberg, P., et al., 2005a, MNRAS, 356, 1155 (astro-ph/0407537)
Croton, D.J., Springel, V., White, S.D.M. et al. 2005b, MNRAS, (astro-ph/0508046)
Doroshkevich, A., Tucker, D.L., Fong, R. et al. 2001, MNRAS, 322, 369
Doroshkevich, A., Tucker, D.L., Allam, S. Way, M.J., 2004, A&A, 418, 7
Einasto, J., Einasto, M., Hütsi, G., et al. , 2003a, A&A 410, 425 (E03a)
Einasto, J., Einasto, M., Tago, E. et al. 2006a, A&A, (submitted, Paper I) (astro-ph/0603764)
Einasto, J., Hütsi, G., Einasto, M., et al. , 2003b, A&A, 405, 425 (E03b)
Einasto, J., Jõeveer, M. & Saar, E. 1980, MNRAS, 193, 353
Einasto, J., Saar, E., Hütsi, et al. 2006b, (in preparation)
Einasto, J., Tago E., Einasto, M., et al. 2005b, A&A, 439, 45 (E05b)
Einasto, M., Einasto, J., Müller, V., Heinämäki, P., Tucker, D.L. 2003c, A&A, 401, 851
Einasto, M., Einasto, J., Tago, E., Dalton, G. & Andernach, H., 1994, MNRAS, 269, 301 (E94)
Einasto, M., Einasto, J., Tago, E., Müller, V. & Andernach, H., 2001, AJ, 122, 2222 (E01)
Einasto, M., Einasto, J., Tago, E., et al. 2006c; A&A (in preparation) (E06c)
Einasto, M., Tago, E., Jaaniste, J., Einasto, J. & Andernach, H., 1997, A&A Suppl., 123, 119 (E97)
Erdogdu, P., Lahav, O., Zaroubi, S. et al. 2004, MNRAS,352, 939
Fleenor, M.C., Rose, J.A., Christiansen, W.A. et al. 2005, AJ, 130, 957 [astro-ph/0512169]
Gao, L., White, S.D.M., Jenkins, A. et al. 2005, MNRAS, 363, 379
Goto, T. et al. 2002, AJ, 123, 1825
Gott, J.R., Juric, M., Schleger, D. et al. 2005, ApJ, 624, 463 (astro-ph/0310571)
Gregory, S.A. & Thompson, L.A. 1978, ApJ, 222, 784
Ihaka, R., & Gentleman, R., 1996, J. of Computational and Graphical Statistics, 5, 299
Jaaniste, J., Tago, E., Einasto, M. et al. 1998, A&A, 336, 35
Jõeveer, M., Einasto, J. & Tago, E. 1978, MNRAS, 185, 357
Kalinkov, M. & Kuneva, I. 1995, A&A Suppl., 113, 451
Kasun, S.F., & Evrard, A.E. 2004, ApJ, astro-ph/0408056
Klypin, A.A., Einasto, J., Einasto, M. & Saar, E., 1989, MNRAS, 237, 929
Kolokotronis, V., Basilakos, S. & Plionis, M. 2002, MNRAS, 331, 1020; astro-ph/0111044
Korn, G.A. & Korn, T.M. 1961, Mathematical Handbook for Scientist and Engineers, McGraw-Hill Book. Co., Inc.
Lahav, O. 2004, Pub. Astr. Soc. Australia, 21, 404
Lahav, O. 2005, In "Nearby Large-Scale Structures and the Zone of Avoidance", eds. A.P. Fairall, P. Woudt, ASP Conf. Series, 329, 3
Nichol, R.C., Sheth, R.K., Suto, Y., et al. 2006, MNRAS, astro-ph/0602548
Oguri, M., Takahashi, K., Ichiki, K., & Ohno, H. 2004, astro-ph/0410145
Oort, J.H. 1983, Ann. Rev. Astr. Astrophys. 21, 373
Porter, S.C. & Raychaudhury, S. 2005, MNRAS, 364, 1387 [astro-ph/0511050]
Praton, E.A., Melott, A. L. & McKee, M.Q. 1997, ApJ, 479, L1
Proust, D., Quintana, H., Carrasco, E.R. et al. 2006, A&A, 447, 133
Ragone, C.J., Merchan, M., Muriel, H., Zandivarez, A., 2004, MNRAS, 350, 983
Ragone, C.J., Muriel, H., Proust, D. et al. 2006, A&A, 445, 819
Saar, E., Einasto, J., Einasto, M. et al. 2006, (in preparation)
Sahni, V., Sathyaprakash, B.S. & Shandarin, S.F. 1998, ApJ, 495, L5
Shen, J., Abel, T., Mo, H., & Sheth, R.K. 2005, astro-ph/0511365
Sousbie, T., Pichon, C., Courtois, H. et al. 2006, ApJ, astro-ph/0602628
Springel, V., White, S.D.M., Jenkins, A. et al. 2005, Nature, 435, 629; astro-ph/0504097
Tago, E., Einasto, J., Saar, E. et al. 2006, AN (accepted) (T06)
Vogeley, M.S., Hoyle, F., Rojas, R.R. et al. 2004, Proc. IAU Coll. No. 195 (astro-ph/0408583)
Wray, J.J., Bahcall, N., Bode, P. et al. 2006, astro-ph/060306
Zeldovich, Ya.B., Einasto, J., Shandarin, S.F., 1982, Nature 300, 407
Zucca, E. et al. 1993, ApJ, 407, 470